

FAST SERIES RESISTANCE IMAGING USING PHOTOLUMINESCENCE

E. Pink, T. Trupke, R.A. Bardos, M.D. Abbott, Y. Augarten, S. Kontermann¹

Centre of Excellence for Advanced silicon Photovoltaics and Photonics, University of New South Wales Sydney, 2052, NSW, Australia, Tel.: +61 2 9385 4054, Fax: +61 2 9662 4240, email: pinky3@gmail.com

¹Fraunhofer Institute for Solar Energy Systems (ISE), Freiburg, Germany

ABSTRACT: This paper discusses a method for very fast spatially resolved quantitative measurement of the series resistance which is based on luminescence imaging. The application of this technique is demonstrated on a number of mono and multi-crystalline silicon solar cells. The resulting series resistance images highlight various specific solar cell material and processing issues which can cause locally enhanced series resistance. The use of local calibration factors is shown to largely remove the effect of lifetime variations across the cell on the resulting series resistance images taken on multi-crystalline cells. Series resistance images obtained from photoluminescence show good agreement with more established techniques such as Corescan.

Keywords: Photoluminescence, Resistance, Contact

1 INTRODUCTION

The series resistance R_s can be a major factor limiting the efficiency of commercial silicon solar cells. Large lateral variations of the metal-semiconductor contact resistance are often observed in screen printed solar cells, which can be the result e.g. of non ideal firing conditions. Characterization tools are therefore required to measure such lateral variations of the series resistance. Existing methods to measure variations of R_s across silicon solar cells include: R_s -DLIT and R_s -ILIT [1], Corescan [2], CELLO [3], and microwave-PCD [4]. With data acquisition times on the order of ten minutes to hours per cell none of these techniques is currently fast enough for inline process control. Electroluminescence (EL) and Photoluminescence (PL) imaging techniques have recently been introduced as fast characterization tools for silicon solar cells and large area silicon wafers [5, 6]. The influence of lateral series resistance variations on both EL images and on PL images measured with simultaneous current extraction from the cell was demonstrated in [7]. A quantitative method for spatially resolved series resistance imaging (PL- R_s) as well as the feasibility of using PL imaging to obtain quantitative series resistance images with data acquisition times on the order of seconds were demonstrated in [8]. More recently a combination of EL imaging and lock-in thermography was also proposed as a way to measure R_s variations[9].

Here, we apply the PL- R_s technique to a variety of different cell types and compare the results to Corescan measurements on the same cells.

2 BACKGROUND

2.1 Theory

The theory of quantitative PL resistance imaging is explained elsewhere [8]. In summary, the method is based on the ability to infer a local diode junction voltage U_i from the local emitted luminescence $I_{PL,i}$ via

$$I_{PL,i} = C_i \cdot \exp\left(\frac{eU_i}{kT}\right) \quad (1)$$

where C_i is a local calibration constant. A first image (the calibration image) is taken at open circuit and at low illumination intensity (here we use ~ 0.17 Suns). Eq.1 is

then used to determine local calibration factors C_i from the measured luminescence intensity $I_{PL,i,1}$ and the terminal voltage U_1 measured at that illumination level. A second image is then taken with one Sun equivalent illumination intensity, and with 80-85% of the photo-generated current extracted from the cell, in order to ensure that a large fraction of the generated current flows through the series resistances $R_{s,i}$. The cell is thus operated near the maximum power point during the measurement of the second image. The local diode voltages $U_{i,2}$ during the second measurement are then evaluated from the local luminescence intensities $I_{PL,i,2}$ and the terminal voltage U_2 using Eq.1. The voltage drop across the local series resistance $\Delta U_{R_{s,i}}$ is then given as the difference between the terminal voltage U_2 and the local diode voltage $U_{i,2}$, i.e.

$$\Delta U_{R_{s,i}} = U_2 - U_{i,2} = U_2 - kT \cdot \ln\left(\frac{I_{PL,i,2}}{C_i}\right) \quad (2)$$

The C_i calibration factors determined from the first image are used for the calculation of $\Delta U_{R_{s,i}}$ via Eq.2 and are dependant on the optical transmittance, reflectance and haze of the front and rear surfaces as well as on the recombination-diffusion parameters L_e , D_e , S_e . The injection level in the cell during the second imaging is similar to the open circuited cell at 0.17 suns, minimizing any effect arising from the injection level dependences of L_e , and S_e .

The local series resistance is given as

$$R_{s,i} = \frac{\Delta U_{R_{s,i}}}{J_i} \quad (3)$$

The local current density J_i is estimated using

$$J_i = J_{SC} - J_0 \cdot \exp\left(\frac{eU_i}{kT}\right) = J_{SC} - J_0 \cdot \frac{I_{PL,i}}{C_i} \quad (4)$$

where the dark current density per unit area J_0 is evaluated from the 1 sun IV curve. An advantage of measuring the PL image with current extraction with a large fraction of the photocurrent being extracted is that variations of J_0 then have a much smaller impact on the local current density.

2.2 Short Circuit Corrections

PL images taken under illumination and with a large fraction of the photocurrent extracted do not obey Eq.1 because of the diffusion limited lifetime of optically generated carriers in the bulk [8, 10, 11]. This means that

the luminescence intensity emitted upon radiative recombination of the carriers that remain in the bulk as a result of the diffusion limitation is not related to the carrier density near the junction via Eq.1.

Theoretical modelling shows that depending on the wavelength used and recombination-diffusion parameters, as much as 50% of the measured luminescence intensity can be caused by the diffusion limited carrier density, which is independent of the diode voltage [11]. In [8] it was therefore proposed to eliminate the influence of the diffusion limited lifetime by subtracting a PL image measured under short circuit conditions from measurements taken at other operating points. This way a corrected PL signal is obtained that is a more reliable indicator of the diode voltage via Eq.1 over a wider range of voltages.

3 METHODS

PL- R_s measurements as outlined above were performed on a variety of silicon solar cells. An 815nm laser was used to illuminate 6-inch solar cells with up to 1 Sun equivalent illumination homogeneously. A thermoelectrically cooled silicon CCD camera was used to capture luminescence images.

All images were recorded using an illumination intensity sufficient to generate a short circuit current in the cells that is equivalent to 0.17 Suns for calibration images and to 1 sun for current extraction images (except for the Laser Fired Contact (LFC) cell [12] for which we used 1 sun illumination intensity for both images). For series resistance images determined using photoluminescence (PL- R_s), the colour bar shows area specific series resistance in $\Omega.cm^2$. Corescan measurements were performed on the same cells for comparison. In that case the area specific resistances in $\Omega.cm^2$ were calculated from Corescan voltage maps ($V_{ce,i}$) and the short circuit current density J_{SC} using

$$R_{S,i} = 1.8 \frac{V_{ce,i}}{J_{SC}} \quad (5)$$

The ‘correction factor’ of 1.8 was used here as described in [13].

All cells were imaged with a spatial resolution of 160 μm per pixel. Note that the images appear with somewhat reduced image quality and resolution in this paper. A higher resolution version of the paper is available from the corresponding author upon request.

4 RESULTS

4.1 Monocrystalline cell with high fill factor

Figs.1 and 2 show PL- R_s and Corescan images respectively, of an industrial screen printed monocrystalline 6-inch solar cell. The cell has a factor of 77% and is affected only in a minor way by series resistance variations. Most of the cell area is approximately $1\Omega.cm^2$ in the PL- R_s image from Fig.1, a value that is typical for industrial screen printed cells.

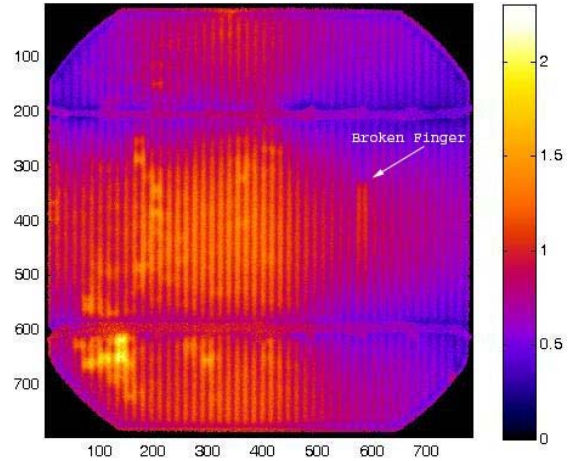


Figure 1: PL- R_s image of a screen printed monocrystalline silicon solar cell with 77% fill factor. Total data acquisition time 4s, resolution 160 μm per pixel.

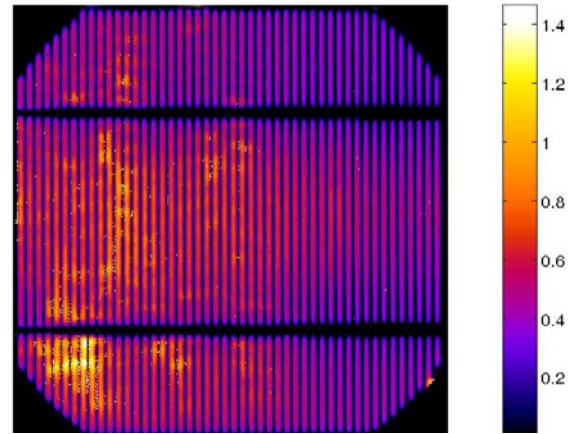


Figure 2: Corescan image of the cell from Fig.1, $J_{SC}=30$ mA/cm², measurement time 33min, 0.5mm spacing between scan lines

Good agreement is observed between the two measurements, with most features visible in both images. A broken finger is clearly visible in the PL- R_s image which is much more difficult to identify in the Corescan image. Why the Corescan does not show the broken finger is not understood. PL- R_s on several cells from this batch showed the broken finger in the same position, pointing to a possible defect in the screen used for printing.

Comparing Figs 1 and 2 shows that the values Corescan reports for the series resistance (between 0.2 and $0.5\Omega.cm^2$ in the low R_s regions) are in general lower than those reported by PL- R_s . One possible explanation for that is that PL- R_s measures the combined effect of the front and rear contact, whereas Corescan is insensitive to R_s variations occurring on the rear, as will be discussed below.

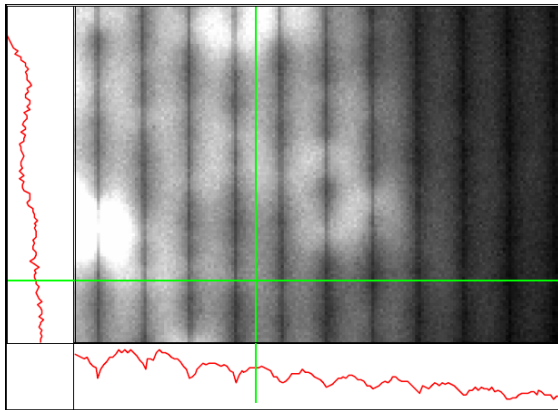


Figure 3: Section from a PL- R_s image of a multicrystalline screen printed solar cell. The cross section at the bottom shows the influence of the emitter sheet resistance.

As has been demonstrated previously with Corescan measurements, the PL- R_s images also show the effects of nonzero sheet resistance. Fig.3 shows a section of a PL- R_s image. The emitter resistance results in the periodic variation of the signal that is visible in the horizontal cross section shown at the bottom of Fig.3. The actual values of R_s reported for emitter resistances should be understood only qualitatively since the resistance added by the emitter is a “distributed” resistance rather than non-distributed ‘lumped’ resistance such as contact resistance.

4.2 Effect of post-annealing on Monocrystalline Cells

The potential negative influence of this annealing step on the front side contact resistance was studied with PL- R_s . Fig.4 shows a PL- R_s image measured on a monocrystalline cell from that study after the annealing step. The cell had a fill factor of 78.0 % prior to the anneal.

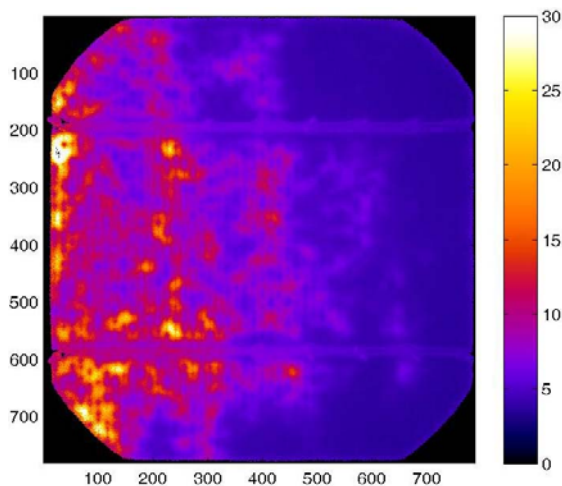


Figure 4: PL- R_s image of a monocrystalline screen printed cell after annealing at 450 °C for 5 minutes. Total data acquisition time 4s.

Annealing for 5 minutes at 450 °C reduced the fill factor to 53%. The PL- R_s image reveals a non-homogeneous R_s distribution with a large high R_s -area on the left hand side of the cell. Good agreement with a Corescan

measurement on the same cell was observed. Many cells in the batch showed very similar features, some of them more clearly exhibiting high R_s regions in a pattern that matches the shape of the furnace belt.

4.3 Multicrystalline cell

Fig.5 shows the PL- R_s image of an industrial screen printed multicrystalline cell with low fill factor. For comparison, a PL-OC image is shown in Fig.6. Most of the cell has values of $R_{S,i}$ around $1\Omega\cdot\text{cm}^2$. The open circuit PL image in Fig.6 shows lifetime variations in that cell, which can be caused e.g. by grain boundaries, dislocation clusters or other defects. None of those features are visible in the resistance image (Fig.5). This shows that the approach used here of using local calibration factors determined from a separate image effectively eliminates lifetime variations from the series resistance image. In this cell the series resistance problem is localized inside a single large grain in the middle-left of the cell.

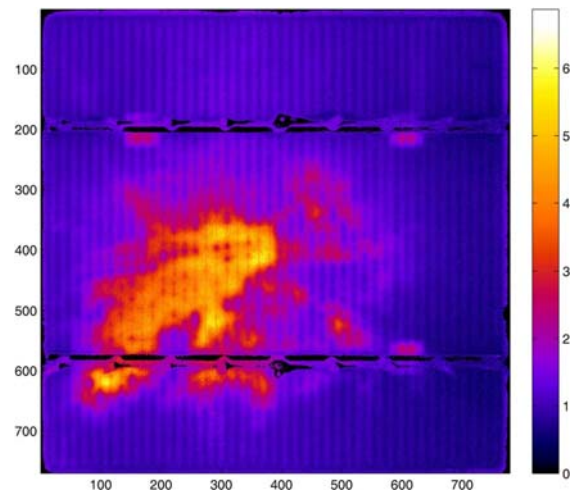


Figure 5: PL- R_s image of a multicrystalline screen printed solar cell with low FF showing a large grain with high R_s .

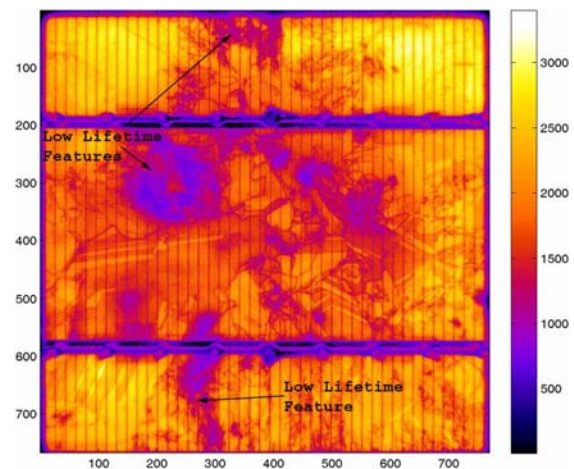


Figure 6: PL image of the cell from Fig.5 measured under open circuit conditions. Measurement time 1s. the colour bar gives the measured intensity in counts per second per pixel.

The outline of the grain is visible in Fig.6. Van der Heide

et al. have observed that grains oriented near the $\langle 100 \rangle$ direction in mc-Si solar cells made from alkaline saw-damage etched wafers have very large contact resistances [14] which may be the cause for the large contact resistance in this grain.

4.4 Firing belt patterns

Fig.7 shows a PL- R_s image of a cell which had a fillfactor of $FF = 78.3\%$ after firing. This cell was then annealed for 10 minutes at 400°C , resulting in a significantly lower fill factor of 64% .

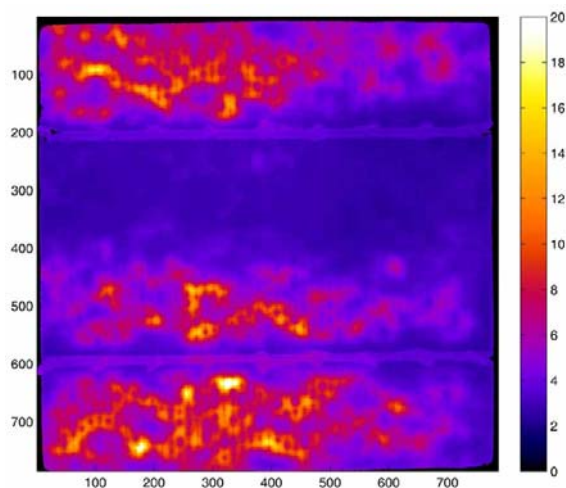


Figure 7: PL- R_s image of a multicrystalline solar cell showing furnace belt features

Severe non-uniformity of R_s is present, with a significant proportion of the cell area above $6 \Omega\cdot\text{cm}^2$. The features resemble the pattern of the belt from the firing furnace. As the solar cell is heating by lamps from above and below during firing, shading by the belt could result in temperature gradients on the cell. This will yield areas of underfired contacts that are more sensitive to annealing [15].

4.5 Laser fired contact cell - rear contact problems

Laser-Fired Contact cells and interdigitated rear contact cells are examples of cell concepts that require characterization techniques allowing both front and rear contact series resistance variations to be measured. Figs.8 and 9 show a PL- R_s image and a Corescan image, respectively, of a LFC cell which has a very poor fill factor ($\sim 40\%$) due to high contact resistance at the rear (normal LFC cells show FF 's similar to standard back surface field cells).

Because of its extremely high resistance, the normal PL- R_s procedure had to be slightly modified to obtain a reasonable R_s image, i.e. the calibration factors were determined at a higher injection level. Fig.8 shows very high resistances ($>20\Omega\cdot\text{cm}^2$) over much of the cell surface, and many small localised points of improved contact resistance are observed across the surface. In contrast to previously reported results these point like features are not aligned with the front grid fingers, which points to a series resistance effect occurring on the rear surface. This is supported by the fact that none of these features are observed in the Corescan measurement. The point like features are currently thought to be related to individual laser pulses from the LFC process. It is

unclear at this stage why only relatively few laser pulses have actually formed good contacts.

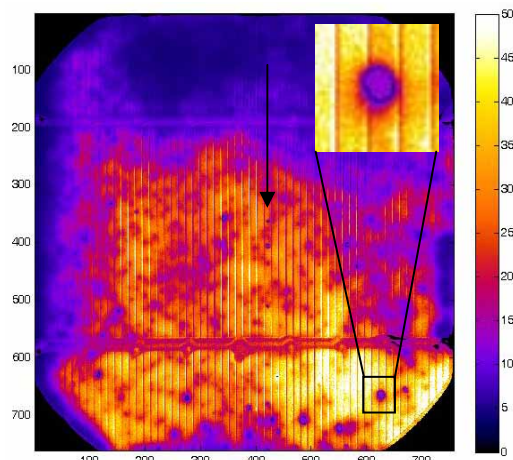


Figure 8: PL- R_s of a monocrystalline laser-fired contact cell.

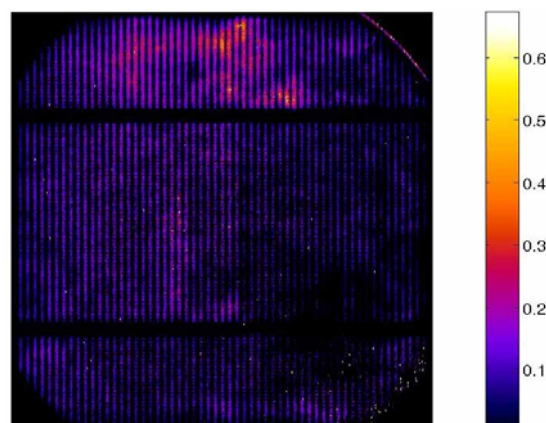


Figure 9: Corescan, of the LFC cell from Fig.8, measurement time 33mins, 0.5mm line spacing, current density $30\text{mA}/\text{cm}^2$.

It can also be seen that the values reported by Corescan in Fig.9 are unrealistically low, between 0.05 and $0.35\Omega\cdot\text{cm}^2$. This may be due to the extremely high values of resistance from the rear surface. This may be due to the extremely high series resistance of the cell's rear affecting the actual current density flowing, lowering the cell J_{sc} . If the current is overestimated, then the calculated resistance will be underestimated. The $30\text{mA}/\text{cm}^2$ current density used in the measurement was not optimal for such a high resistance and the measurement would have been more accurate using $10\text{mA}/\text{cm}^2$.

4.6 Lifetime variations

A PL image of another LFC cell measured under open circuit conditions is presented in Fig.10. The image shows the presence of a large circular lifetime feature, the shape of which may be caused e.g. by a sample holder of the same size and shape. Using the quantitative methodology described above these substantial lifetime variations are effectively removed from the PL- R_s image of the same cell as shown in Fig.11.

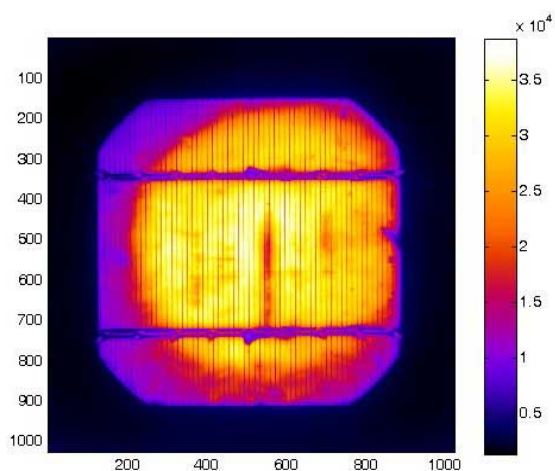


Figure 10: Open Circuit PL image measured with one Sun equivalent illumination intensity showing a circular lifetime feature.

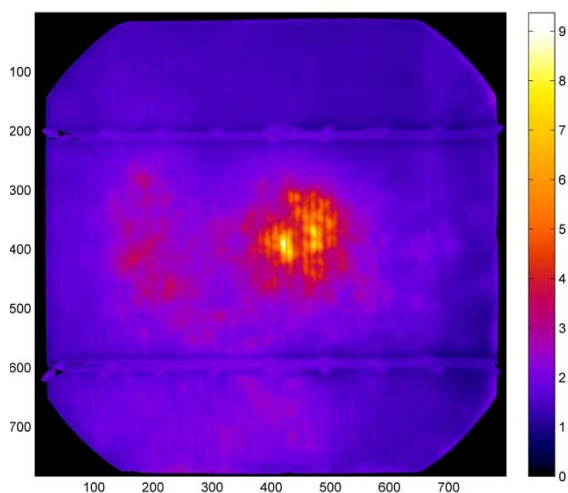


Figure 11: PL- R_s of the cell from Fig.10. The influence of the dominating lifetime feature in that image is eliminated from the PL- R_s image.

5 CONCLUSIONS

Photoluminescence-based series resistance imaging (PL- R_s) is successfully applied to a number of different types of silicon solar cells. The ability to eliminate errors caused by lifetime variations in these images has been demonstrated, which is particularly important for screen printed solar cells. Measurements on LFC cells revealed series resistance variations form the rear surface that are not detected by Corescan. In most cases it is easy to identify, whether the dominating R_s effects in any given cell arise from the front or from the rear contact. In cases where this is not possible the comparison with Corescan is useful as Corescan only measures front contact resistance problems.

The full quantitative PL- R_s analysis used here involves four separate images to be measured. On most cells presented here these four measurements were carried out with 1s exposure time each, resulting in 4s total data acquisition time. Qualitative R_s images can be measured

in 1s, which makes this technique attractive for inline process control.

For series resistance values $<5\Omega\text{cm}^2$ our method is estimated to provide the spatially resolved series resistance with $<20\%$ relative error. At very high series resistance values the error becomes larger. In that case a variation of the methodology discussed here, which will be discussed elsewhere (i.e. a different combination of images) should give more reliable quantitative data.

ACKNOWLEDGEMENT

The Centre of Excellence for Advanced Silicon Photovoltaics and Photonics is supported under the Australian Research Council's Centres of Excellence Scheme.

REFERENCES

- [1] O. Breitenstein, J.P. Rakotoniaina, A.S.H.v.d. Heide, and J. Carstensen, *Progress in Photovoltaics* **13** (2005) 645.
- [2] A.S.H.v.d. Heide, J.H. Bultmann, J. Hoornstra, and A. Schönecker, *Proceedings of the 17th EPVSC, Munich* (2001) 1531.
- [3] J. Carstensen, G. Popkirov, J. Bahr, and H. Föll, *Solar Energy Materials and Solar Cells* **76** (2003) 599.
- [4] C. Ballif, S. Peters, and D. Borchert, *Progress in Photovoltaics* **11** (2003) 309.
- [5] T. Fuyuki, H. Kondo, Y. Kaji, T. Yamazaki, Y. Takahashi, and Y. Uraoka, *31st IEEE Photovoltaic Specialists Conference, Orlando, USA* (2005).
- [6] T. Trupke, R.A. Bardos, M.C. Schubert, and W. Warta, *Applied Physics Letters* **89** (2006) 044107.
- [7] T. Trupke, R.A. Bardos, M.D. Abbott, F.W. Chen, J.E. Cotter, and A. Lorenz, *WCPEC-4, Waikoloa, USA* (2006).
- [8] T. Trupke, E. Pink, R.A. Bardos, and M.D. Abbott, *Appl. Phys. Lett.* **90** (2007) 093506.
- [9] K. Ramspeck, K. Bothe, D. Hinken, B. Fischer, J. Schmidt, and R. Brendel, *Applied Physics Letters* **90**(15) (2007) 153502.
- [10] M.D. Abbott, R.A. Bardos, T. Trupke, K.C. Fisher, and E. Pink, *Journal of Applied Physics* **102**(4) (2007) 044502.
- [11] M. Kasemann, D. Grote, B. Walter, T. Trupke, Y. Augarten, R.A. Bardos, E. Pink, M.D. Abbott, and W. Warta, *this conference*.
- [12] E. Schneiderlöchner, R. Preu, R. Lüdemann, and S.W. Glunz, *Progress in Photovoltaics* **10**(1) (2002) 29-34.
- [13] Corescan manual, p.14; http://www.mechatronics.nl/support/user/download/USER_MRN_061_CoRRescan_printable%20version.pdf
- [14] A.v.d. Heide, J. Bultman, M. Goris, and J. Hoornstra, *WCPEC-3, Osaka, Japan*, (2003) 1036.
- [15] S. Kontermann, D. Reinwand, A. Grohe, D. Erath, R. Preu, G. Willeke, E. Pink, and T. Trupke, *this conference*.